Soils and Foundations 2014;54(2):81–93

The Japanese Geotechnical Society

Soils and Foundations

www.sciencedirect.com
journal homepage: www.elsevier.com/locate/sandf

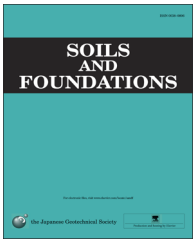

Unloading behavior of clays measured by CRS test

Hiroyuki Tanaka[a,*], Ayato Tsutsumi[b], Taro Ohashi[c]

[a]*Division of Field Engineering for the Environment, Graduate School of Engineering, Hokkaido University, Japan*
[b]*Research Institute, Penta Ocean Construction, Japan*
[c]*Sapporo City Government, Japan*

Received 11 June 2012; received in revised form 13 September 2013; accepted 1 October 2013
Available online 13 March 2014

Abstract

The unloading behavior of clays was studied by the Constant Rate of Strain (CRS) test, for three clays: two of them are reconstituted and the other was intact. In the conventional CRS test where the stress monotonically increases, the distribution of the pore water pressure in a specimen is assumed to be parabolic, the effective stress is calculated and then the compression behavior is evaluated. However, this assumption cannot be directly applied the unloading condition. In this study, the pore pressure distribution under unloading was simulated by a cubic polynomial under the assumption that hydraulic conductivity does not change in the unloading process. A unique relation in the e–log σ'_v relation was found, irrespective of both the magnitude of stress or strain and the compression index, C_c, at the unloading test, when the consolidation pressure is normalized by σ'_{vmax}, which is the consolidation pressure before the unloading test. In addition, the creep strain, which is gained by constant loading before the unloading test, was shown to have a great effect on the unloading behavior: that is, the soil behaves stiffly when subjected to a constant load for a prolonged period of time. A strain rate dependency in the unloading process was also observed particularly for heavily unloaded specimens. The unloading behavior was also investigated by the conventional constant load test. The test results show reasonable agreement with those obtained from the CRS test.

Keywords: Unloading; One-dimensional consolidation; Creep; Strain rate effect; IGC: D5

1. Introduction

The swelling index (C_s) is a key parameter in geotechnical engineering, as well as the compression index (C_c). C_s may be defined as the slope of the relation between the void ratio (e) and the consolidation stress (σ_v) in the common logarithm scale (in the Cam Clay model, κ is used in the natural logarithm scale, ln σ_v). Characteristics of C_s or κ have been investigated by many researchers and used for the prediction of shear strength (see for example, Mitachi and Kitago, 1976; Ohta et al., 1985; Wood, 1990) or shear modulus (for example, Kawaguchi and Tanaka, 2008). C_s is usually measured by a constant loading oedometer test or triaxial tests, where applied stresses decrease step by step, and the negative excess pore water pressure caused by unloading is dissipated through drainage boundaries.

Unlike conventional tests for obtaining C_c, i.e., increasing loading stress, the testing method for C_s is not strictly defined. For example, various load removal decrement ratios have been adopted and in an extreme case as the previous Japanese

*Corresponding author.
E-mail address: tanaka@eng.hokudai.ac.jp (H. Tanaka).
Peer review under responsibility of The Japanese Geotechnical Society.

Production and hosting by Elsevier

http://dx.doi.org/10.1016/j.sandf.2014.02.001
0038-0806

Table 1
Geotechnical properties for tested soils in this study.

Sample	ρ_s (g/cm^3)	w_n (%)	w_L (%)	w_P (%)	I_p	c_v (cm^2/d)	k (m/s)	Remarks
Kasaoka	2.610	45.8	62	36	26	39	7×10^{-11}	Recons.
Louiseville	2.769	69.4	74	23	51	110	3×10^{-10}	Intact
Ma13	2.693	73.6	91	38	53	83	3×10^{-10}	Recons.

Industrial Standards (JIS) for incremental loading test (JIS A 1217:1990), C_s was obtained from the change in the void ratio from the final to the first loading stage. In this standard, with eight loading stages and a load increment ratio of one, the decrement ratio for C_s can be as small as 0.0078. This specification was, however, eliminated in the present JIS (JIS A 1217:2009) on the basis that C_s is strongly affected by the decrement ratio. This point will be discussed in this paper. A duration of 24 h is usually adopted for the constant loading test although there is no theoretical reason for doing so. This is probably because it is convenient for those who conduct the experiments. A reason for employing such loosely defined testing methods may be that it is commonly believed that soil under unloading behaves elastically and only the dissipation of the negative pore water pressure should be considered. However, Mesri et al. (1978) studied unloading behavior using the constant loading oedometer and triaxial equipments, and revealed that C_s is not a constant parameter, but is rather strongly influenced by the stress levels and also that the effect of creep (secondary compression) is significant at large stress removals.

The Constant Rate of Strain (CRS) oedometer provides constant strains to a specimen, instead of the constant loads in the conventional oedometer test, and has gradually come into use as a routine test to measure the compression behavior of soft clays. One of the starting points for the wide use of CRS in Japan may have been the investigation of compressibility for Pleistocene clay layers for the construction of the Kansai International Airport (KIA). Due to the large burden pressure, the yield consolidation stress (σ_{vy}) for these Pleistocene clay layers cannot be accurately measured by the conventional oedometer test, where the increment of the magnitude of load in each step is the same as at the previous loading step. In CRS test, however, the e–log σ_v relation can be almost continuously measured so that the σ_{vy} value can be clearly defined. Another advantage in the CRS test is that the rate effect on the e–log σ_v relation can be considered directly. Since the final consolidation stress caused by the weight of the manmade island in the Pleistocene clay layers at KIA is very close to the σ_{vy} value, the rate effect greatly influences the prediction of the settlement (for example, see Tanaka, 2005; Watabe et al., 2008). On the other hand, due to the small amount of displacement in the unloading process, it was considered that the CRS test is not suitable for obtaining unloading behavior. Tsutsumi and Tanaka (2011) have developed a new loading apparatus for the CRS test, which provides precise displacements using a step motor controlled by a computer. This paper will present the unloading behavior measured by this CRS test.

2. Tested samples and testing method

2.1. Soil sample

Three kinds of soil samples were prepared in this study, as indicated in Table 1. Two of the samples (Kasaoka and Ma13) were reconstituted, and the Louiseville clay was an intact sample. Kasaoka clay is commercially available powder clay. Ma13 clay is a natural Holocene clay collected from Osaka bay. These clay samples were thoroughly mixed with water at about 2 times their liquid limit (w_L) and consolidated in a cell under 100 kPa consolidation pressure. After consolidation was completed, the samples were extruded from the cell and were wrapped with plastic film and covered by wax. Then the samples were stored in a box under high humidity and constant temperature until testing. The natural water content (w_n) in Table 1 is the water content after extrusion from the consolidation cell. Louiseville clay samples were retrieved at the site of Louiseville, Quebec, Canada, following the Japanese standard sampling method using the Japanese standard sampler. Although the main properties of this clay have been reported by Leroueil (1997) and Tanaka et al. (2001), the most prominent consolidation characteristic is non-linearity in the e–log σ_v relation, as shown in Fig. 1. A sharp reduction in the e–log σ_v relation after σ_{vy} is observed and its gradient gradually becomes moderate as σ_v increases. Because of reconstituted samples of Kasaoka and Ma 13 clay, the e–log σ_v relation is almost linear in the normally consolidated (NC) state, as shown in Fig. 1. The most significant difference between these reconstituted samples is their permeability, as shown in Table 1, where the coefficient of consolidation (c_v) and the hydraulic conductivity (k) were measured at σ'_v=about 300 kPa.

2.2. Testing method

The testing apparatus used in this study is the same as that used in previous research (Tsutsumi and Tanaka, 2011), except for a gap sensor to make precise measurements of displacement. The capacity of this gap sensor is 2 mm, and its resolution is 0.0001 mm but considering the noise yielded in the recoding and amplifier systems, accuracy is reliable to about 0.0005 mm. The specimen was 60 mm in diameter and 20 mm in initial height. The upper side of the specimen was kept drained and the pore water pressure (u) was measured at the bottom (u_b). A back pressure of 100 kPa was applied to allow for precise measurements of the pore water pressure.

3. Pore water pressure distribution in the specimen

Fig. 1 shows the e–log σ_v relation and stress levels for unloading tests. Several unloading tests were carried out for a specimen at the NC state where the consolidation stress considerably exceeds the σ_{vy} value so that the influence of the bedding error caused by the roughness of both sides of the specimen can be avoided. Also, u_b can be precisely measured because the large amount of deformation left no clearance between the specimen and the oedometer ring. Several steps of stress reduction can be noted in the unloading tests in Fig. 1. This was caused by the suspension of the loading apparatus to set up the gap sensor, because of its small capacity.

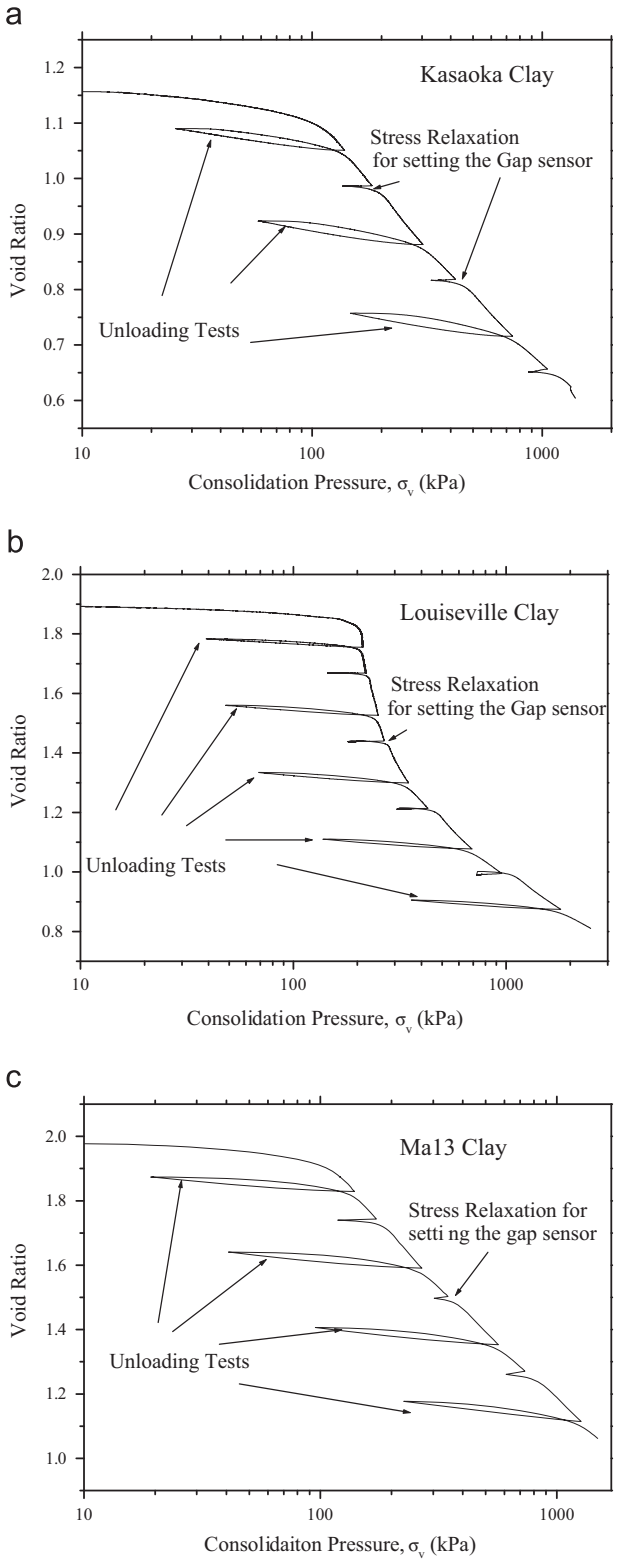

Fig. 1. e–log σ'_v relation for tested clays and stress levels of unloading tests. (a) Kasaoka Clay, (b) Louiseville clay, and (c) Ma13 clay.

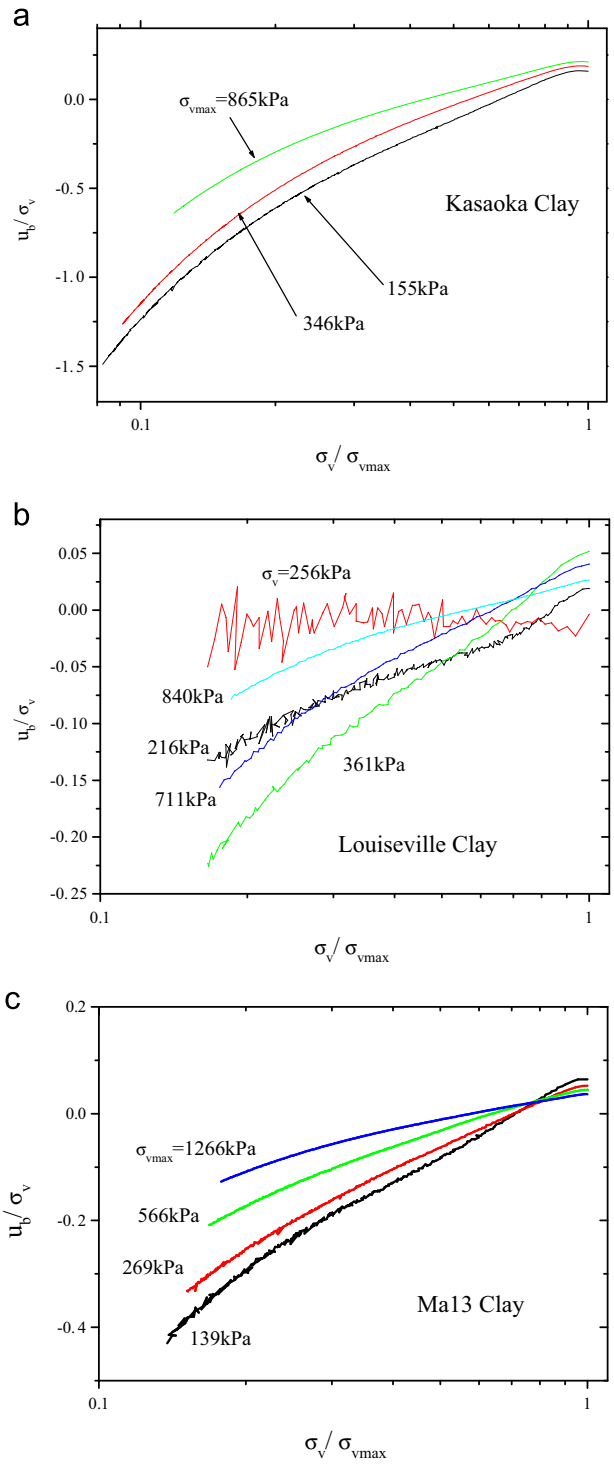

Fig. 2. Pore water pressure measured at the bottom during the unloading test. (a) Kasaoka Clay, (b) Luiseville Clay, and (c) Ma13 clay.

Fig. 2 shows the pore water pressure generated by the unloading, as measured at the bottom of the specimen (u_b), and u_b is normalized by the consolidation stress, as (u_b/σ_v). In these figures, σ_{vmax} is the stress before the unloading test. u_b/σ_v gradually decreases as σ_v decreases, and at the final stage, the order of (u_b/σ_v) drops as low as -1.5 for $\sigma_{vmax}=155$ kPa for Kasaoka clay; that is, the absolute u_b value is 1.5 times that of the current consolidation stress (σ_v). In Figs. 1 and 2, both σ_v and σ_{vmax} were measured directly by the load cell attached to the shaft, and were not corrected by the generated pore water pressure. It should be noted that values of u_b/σ_v are too large to ignore the excess pore water pressure for characterizing unloading behavior in terms of the effective stress.

Since the pore water pressure is continuously generated in the specimen in the CRS test, the stress measured by the load cell needs to be interpreted in terms of effective stress. Usually in CRS tests, the effective consolidation stress (σ'_v) is calculated by Eq. (1) from σ_v and u_b according to the fact that pore water pressure is distributed in a parabolic manner (Moriwaki and Umehara, 2003). Although the value of σ'_v varies with location in the specimen, the representative value of σ'_v adopted is the average of the σ'_v values in the specimen.

$$\sigma'_v = \sigma_v - \frac{2}{3}u_b \tag{1}$$

However, this calculation method cannot be applied to tests for unloading or when the strain rate drastically changes. To study the distribution of u during the unloading, an FEM analysis was carried out based on the Cam Clay model with soil parameters as indicated in Table 2. The boundary conditions and applied stress over time are shown in Fig. 3. The compression and swelling indices, λ and κ, were 0.2 and 0.04, respectively. The initial void ratio (e_o) is 1.2 at $\sigma'_{vo}=30$ kPa, which is the effective burden stress before loading. The amount of consolidation stress ($\Delta\sigma_v$) applied was 100 kPa (the final consolidation stress became 130 kPa). Hydraulic conductivity (k) decreased with decreasing e, as shown in the following

$$k = k_0 + \lambda_k \ln\left(\frac{e}{e_0}\right) \tag{2}$$

where, k_o is k at e_o, λ_k is a coefficient of k against e.

The calculated results are shown in Fig. 4 ($y/H=0$: undrained, $y/H=1.0$: drained), where the degree of consolidation (U) is about 90% with a pore water pressure of 15.5% of $\Delta\sigma_v$ at the bottom. The time factor (T_v) at this time is 1.29, where T_v is calculated using the average compressibility coefficient (m_v) and k between σ'_{vo} and ($\sigma'_{vo}+\Delta\sigma_v$). Fig. 4 shows also the distribution of u at ΔT_v of 0.013 after the load is removed by $0.1\Delta\sigma_v$. Although u at the bottom decreases in the nearly same order of the removed stress of $0.1\Delta\sigma_v$, the pore pressures at the layer near the drained surface become

Table 2
Soil parameters used in FEM analysis.

λ	0.2
κ	0.04
e_o	1.2
σ'_{vo} (kPa)	30
$\Delta\sigma_v$ (kPa)	100
k at e_o (m/s)	1.16×10^{-9}
λ_k	0.2

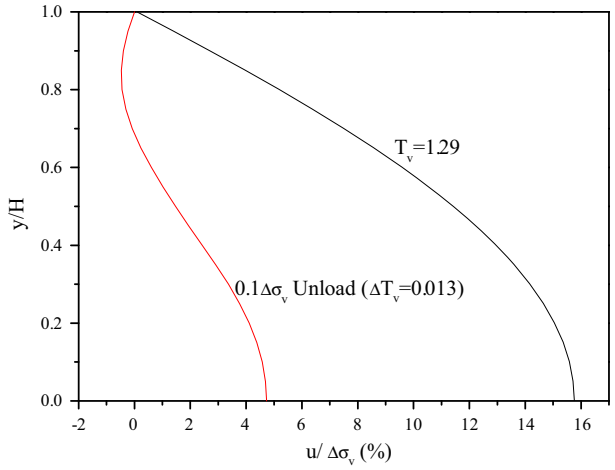

Fig. 4. Distribution of pore water pressure due to unloading (FEM).

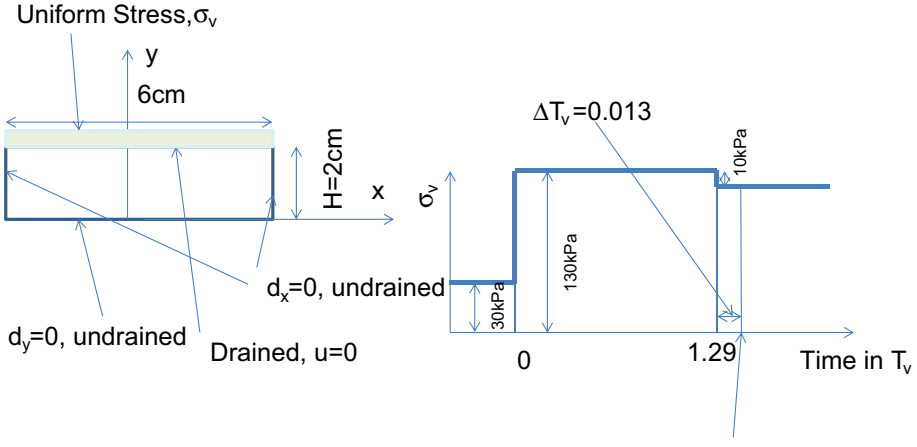

Fig. 3. Boundary conditions and applied stress for FEM.

negative. This is because the soil layer has a tendency to swell due to the reduction of consolidation stress. In the CRS test specimens, it is reasonable to assume the same is taking place in the transit time between loading and unloading.

To find a calculation method to evaluate the effective stress in the specimen during the unloading test, the distribution of the pore water pressure is simulated by the cubic polynomial in

$$u = Ay^3 + By^2 + Cy + D \tag{3}$$

where, A, B, C and D are the constants defined by the following boundary conditions.

$$\text{At } y = 0,\ u = u_b \text{ and } \frac{du}{dy} = 0 \tag{4}$$

$$\text{At } y = H,\ u = 0 \text{ and } \frac{du}{dy} = i\gamma_w \tag{5}$$

where, i is the hydraulic gradient at H and γ_w is the unit weight of water.

From the above boundary conditions, these constants can be expressed by the following equations:

$$A = \frac{2u_b + Hi\gamma_w}{H^3} \tag{6}$$

$$B = -\left(\frac{3u_b}{H^2} + \frac{i\gamma_w}{H}\right) \tag{7}$$

$$C = 0 \tag{8}$$

$$D = u_b \tag{9}$$

A comparison between the u distribution by the FEM and simulated by the cubic polynomial equation is made in Fig. 5, where the i value is inserted directly from the pore water pressure gradient at H in Fig. 4. Except for the pore pressures at depths around $y=0.8H$, the closeness of these two lines indicates that the pore pressure distribution can be assumed to be expressed by the cubic polynomial equation.

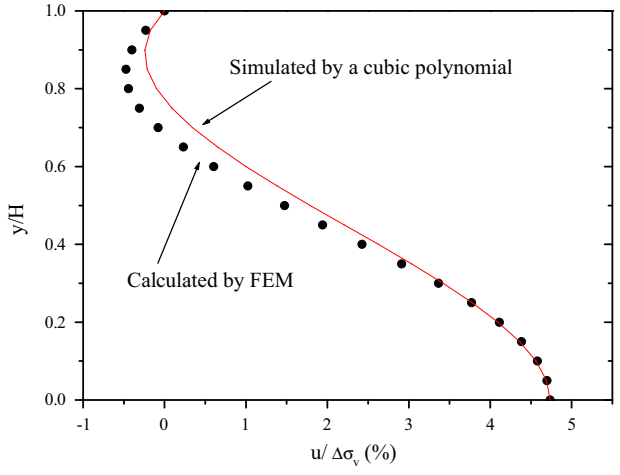

Fig. 5. Comparison of pore water pressure distribution calculated by FEM and simulated by cubic polynomial.

When this assumption is applied to the CRS test, i in Eq. (5) is required. i can be related to the strain rate ($\dot{\varepsilon}$) and k in

$$q = \dot{\varepsilon}h = ki \tag{10}$$

where q is water flow per a unit area and h is the thickness of the specimen.

It may be considered that the change in k during the unloading process is negligible because of the small change in e. Therefore, i is related to only $\dot{\varepsilon}$, i.e., when $\dot{\varepsilon}$ becomes $1/10\dot{\varepsilon}$, i also becomes 1/10 times of that at $\dot{\varepsilon}$. Values of i during the continuously loading process can be easily obtained, assuming that the pore water pressure distribution is parabolic, such as

$$i\gamma_w = \frac{2u_0}{H} \tag{11}$$

where, u_o is the pore water pressure at the bottom during the loading process and to distinguish the pore water pressure during the unloading test (u_b), another symbol u_o will be used. If the unloading test is carried out under the same order of the strain rate at the loading test, i becomes negative without any change in the absolute value.

For imaginarily understanding, the u distribution at several unloading stages is simulated and shown in Fig. 6, based on the observed value of u_b in Kasaoka clay with $\sigma_{vmax}=346$ kPa. u is distributed in a parabolic manner before unloading. However, when the direction of the deformation is changed from compression to swelling, the gradient of u at the drained surface is suddenly reversed. The u_b value decreases partly due to the reduction of the load, but also the dissipation of u. The values of u close to the drained surface are always negative, but with distance from the drained surface, the values are still positive at early stages of the unloading. As σ_v decreases considerably, however, the even the values of u at the bottom become negative.

The average pore water pressure (u_{ave}) in the specimen can be calculated by the integration of Eq. (3), and finally can be defined by

$$u_{ave} = \frac{1}{6}(3u_b + \alpha u_0) \tag{12}$$

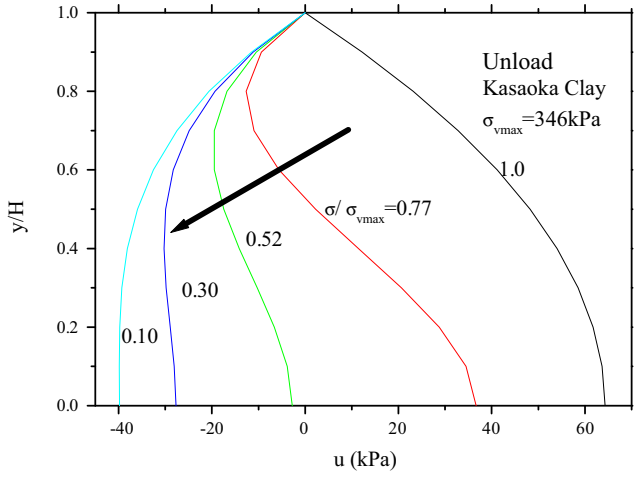

Fig. 6. Change in pore pressure distribution at several unloading stages. Calculation was done based on the pore pressure measured at the bottom for Kasaoka clay.

where α is the coefficient determined by the $\dot{\varepsilon}$ ratio of the present test to the measured u_o: for example, when $\dot{\varepsilon}$ is changed to 1/100 times slower than that at u_o, α becomes 1/00; when the unloading test is carried out under the same absolute strain rate as the previous loading test, α becomes -1.

In the usual continuous loading test, u_{ave} becomes $2/3u_b$, as is the case in Eq. (1) since α is 1 and $u_b = u_o$. In the relaxation test where no strain is generated, u_{ave} is $1/2u_b$, because α is zero. Hereafter, the effective consolidation pressure (σ'_v) is calculated by

$$\sigma'_v = \sigma_v - u_{ave} = \sigma_v - \frac{1}{6}(3u_b + \alpha u_0) \tag{13}$$

4. Unloading behavior

4.1. Normalization of unloading behavior

The e–log σ_v relations measured in the process of the unloading are presented in Fig. 7. In these tests, the strain rate for both loading and unloading is $\pm 3 \times 10^{-6}$/s. In these figures, σ'_{vmax} is normalized by σ'_v just before the unloading; Δe is the increment of e from e at σ'_{vmax}. These figures indicate that the unloading behavior in Δe–σ'_v/σ'_{vmax} relation is uniquely defined, irrespective of the magnitude of σ'_{vmax}. In the case of Ma13 clays, the test results from the constant load tests are also presented: they will be discussed later in this paper. Prior to concluding that the Δe–σ'_v/σ'_{vmax} is independent of the intensity of σ'_{vmax}, the influence of the excess pore water pressure and compliance of the apparatus need to be carefully examined. The former concern is valid when simplifying the pore water pressure to the cubic polynomial, even though the accuracy of this simplification was examined previously (see Fig. 5 for the results). This may be supported by the fact that the uniqueness of the Δe–σ'_v/σ'_{vmax} relation is obtained for soil samples with different levels of u_b due to different values of k (see Table 1), i.e., for Kasaoka and Ma13 clays. Indeed, as shown in Fig. 2, even though the u_b/σ_v ratios for these two clays differ by a factor of 2 or 3, a unique relation between Δe and σ'_v/σ'_{vmax} is observed for both clays.

For the purpose of compliance, the existence of some deformation in the apparatus is inevitably admitted. Displacement for the CRS test was directly controlled by the step motor rather than displacement information from the gap sensor. Some of the displacement generated by the loading apparatus was absorbed by a load cell with relatively high flexibility located between the loading frame and the gap sensor. Therefore, the strain rate at the early stages is not constant. This point will be discussed in more detail in a later section of this paper. One of the problems of this approach is that undetectable displacements are yielded below the gap sensor, due to placing porous metal on the upper end of the specimen, the connections at the pedestal and the loading shaft, etc. It should be kept in mind that because these undetected deformations in this CRS test are proportional to the applied load, they can be expected to be more significant at large stress levels. However, as seen in Fig. 7, where the unloading tests were carried out at

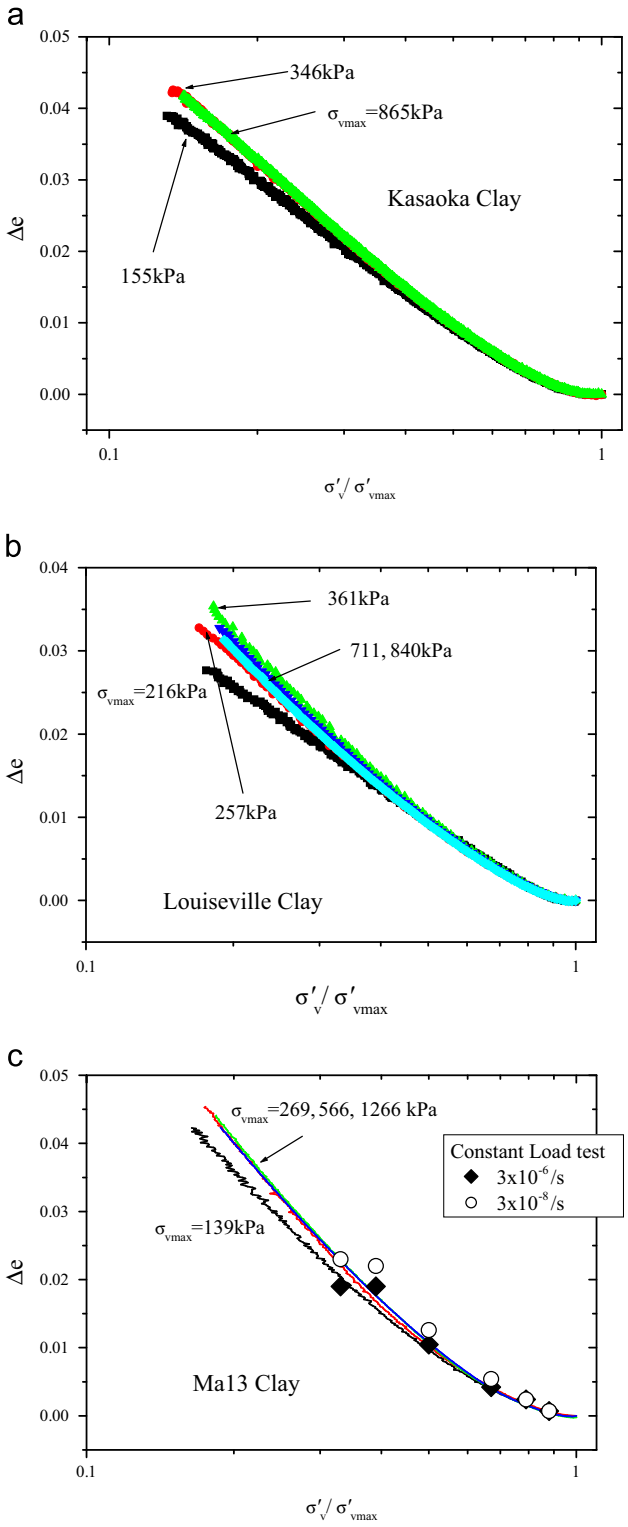

Fig. 7. Normalization of $e - \log \sigma'_v$ relation for the unloading test. (a) Kasaoka Clay, (b) Luiseville Clay, and (c) Ma13 Clay.

different stress levels, the Δe–σ'_v/σ'_{vmax} relation is nearly the same at different σ'_{vmax} levels. This indicates that even though the displacement undetected by the present system cannot be totally ignored, its influence on the Δe–σ'_v/σ'_{vmax} relation seems very small. This inference is also supported by visual analysis, where the displacement of the specimen in the oedometer cell is

observed through a transparent acryl ring by a digital camera and the strain in the specimen is calculated by the displacement of the targets. In an earlier study, Shinohe and Nishimura (2012) concluded that the strain measured by the imaginary analysis and the gap sensor is very similar at relatively large strain levels.

It is interesting to note that even in Louiseville clay, which exhibits strong non linearity in the e–log σ'_v relation at the NC state, the constant Δe–σ'_v/σ'_{vmax} relation is observed, irrespective of different C_c at different stress levels. In many constituted models, especially the Cam Clay, C_s/C_c or κ/λ (including $\Lambda=1-\kappa/\lambda$) is the most fundamental and important parameter. However, the results of the present study indicate that C_s is not related to C_c, but is an inherent value for each soil.

4.2. Influence of creep

Although in this study two reconstituted soils were used, repeatability in the test results is a very important issue, notably because of the very small amount of measured strain during the unloading. However, it was found in the present study that a unique normalization of the Δe - σ'_v/σ'_{vmax} relation is found regardless of the stress and strain levels. Using this useful characteristic, the effect of creep created before the unloading test was studied. At three different σ_v (not σ'_v) levels, i.e., 191, 425 and 1620 kPa for Kasaoka clay, the specimen was subjected to constant σ_v before the unloading test. These stress levels are large enough to erase the histories obtained during the previous unloading test. The duration time of the constant loading was 72, 24 and 12 h for the stress levels, respectively. The constant load was provided by the displacement of the loading apparatus to keep σ_v constant. The variation in the applied stress during the constant load test from the intended σ_v is very small, as shown in Fig. 8. Increase in the strain and dissipation of the pore pressure at the bottom during the constant loading for each stress level is presented in Fig. 9. When the stress level was 1620 kPa, u was not completely dissipated.

Fig. 10 shows the e–σ_v/σ'_{vmax} relations at all the loading and unloading stages; at some stages of the process during the loading, the constant load (creep) and the unloading stages plotted against (Δe_{cr}), and the strain increment when the constant loading test started. The Δe_{cr}–σ'_v/σ'_{vmax} relations with different durations for the constant loading are nearly parallel. It is interesting to note that in order to eliminate the strain caused

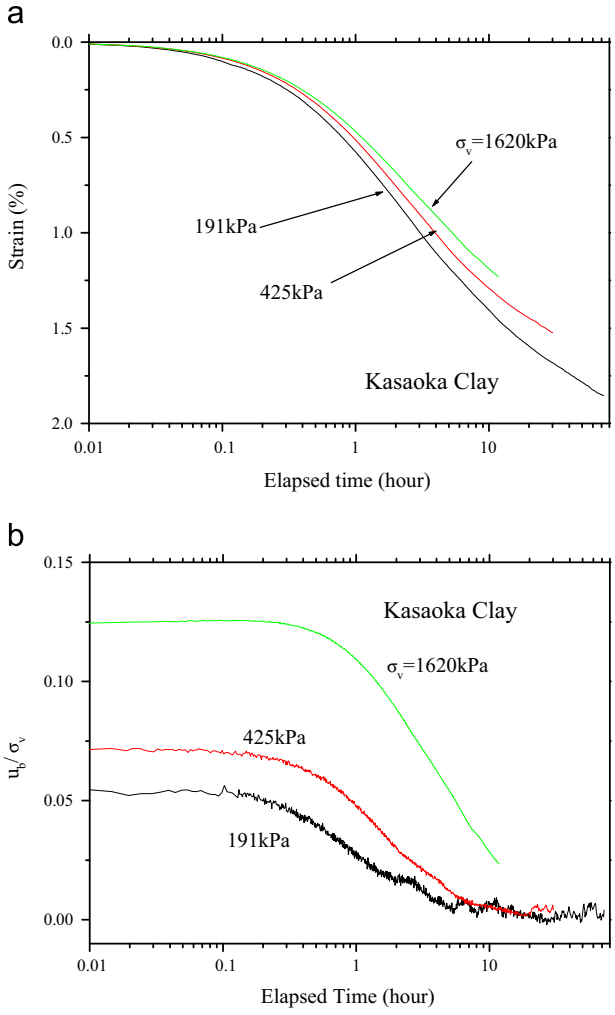

Fig. 9. Consolidation behavior during the constant loading test. (a) Strain and (b) pore pressure measured at the bottom.

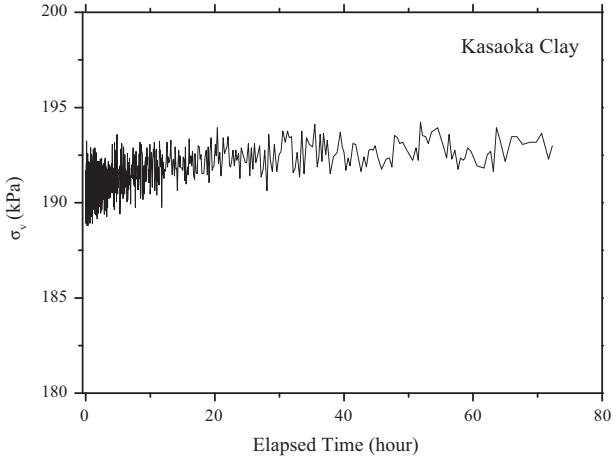

Fig. 8. Variation in the consolidation stress (not effective stress) during the constant loading test.

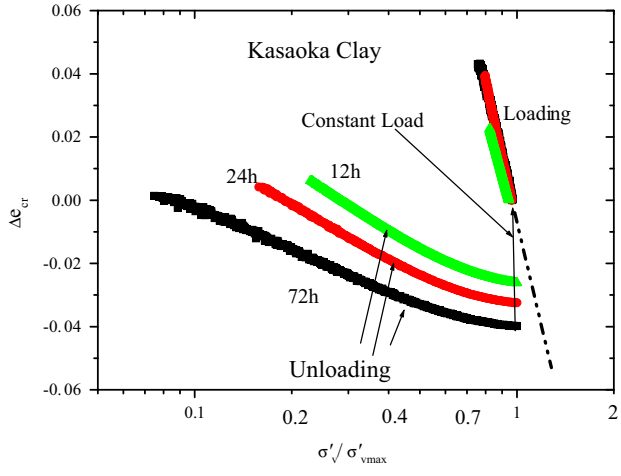

Fig. 10. The unloading test after application of a constant load. The strain (Δe_{cr}) is based on e before applying the constant load.

by the constant loading test, a large portion of the stress needs to be removed; for example, when loading was for 24 h in duration, the intensity was 0.15 times that of the maximum stress.

The Δe–σ'_v/σ'_{vmax} relation for different creep loading times is shown in Fig. 11, where Δe is plotted from the start of the unloading test. The effect of creep strain is clear from the figure: the longer the duration of creep, the flatter the Δe–σ'_v/σ'_{vmax} relation and the smaller the value of C_s. This implies that even under the unloading, the swelling behavior is governed by the strain history.

4.3. Influence of strain rate

To study the rate dependency of the unloading behavior, the strain rate was changed during the unloading test. The testing methods and the test results are shown in Figs. 12 and 13. The points at which the strain rate changed are indicated by letters of the alphabet. The strain rate at the first stage (a and b in the figures) was intended to be a small rate (-3×10^{-8}/s), but this rate was so slow that the strain subjected to the specimen was canceled by the expansion of the load cell due to the decreasing σ_v. As a result, no strain in the specimen was generated in the process of a and b, as was the case in the relaxation test for Kasaoka clay. In Ma13 clay, positive strains (compressive) were generated because the expansion of the load cell was greater that the displacement of loading apparatus (see Fig. 13(a) and (c)). This was consistent with previously reported test results. Fig. 14 shows the strain rates measured by the gap sensor, with and without creep loading before the

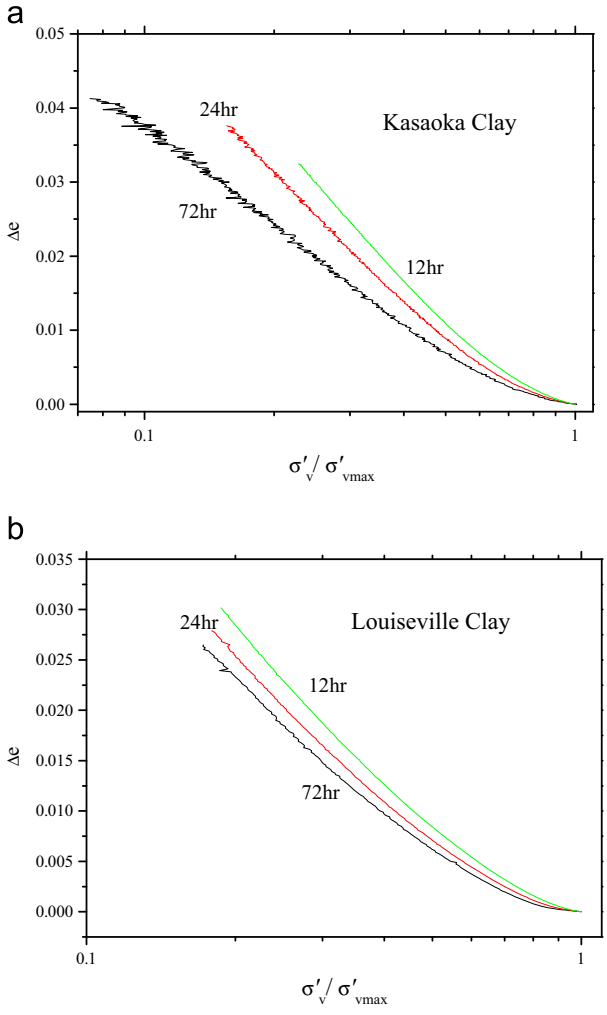

Fig. 11. Comparison of Δe–σ'_v/σ'_{vmax} relations with different duration of the constant load. The strain (Δe) is based on e before the unloading test. (a) Kasaoka Clay and (b) Louiseville Clay.

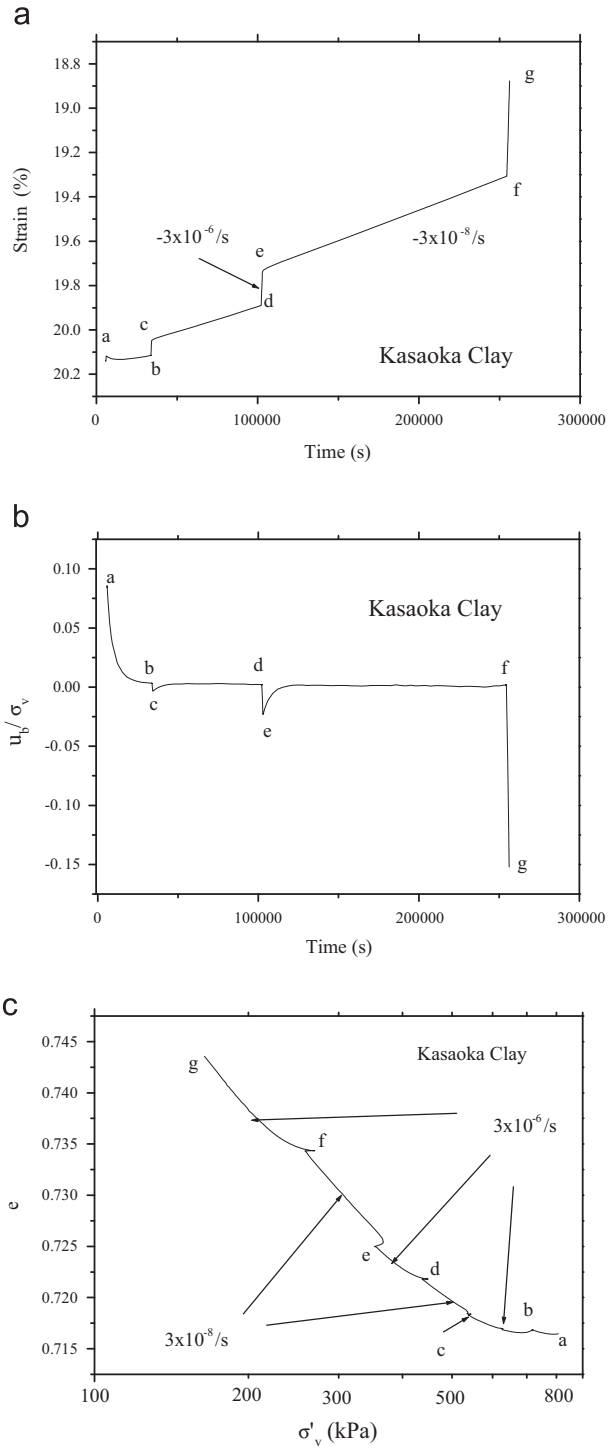

Fig. 12. Influence of the strain rate on the e–log σ'_v relation during the unloading test (Kasaoka Clay). (a) Time vs strain, (b) time vs pore pressure, and (c) e–log p relation at different strain rates.

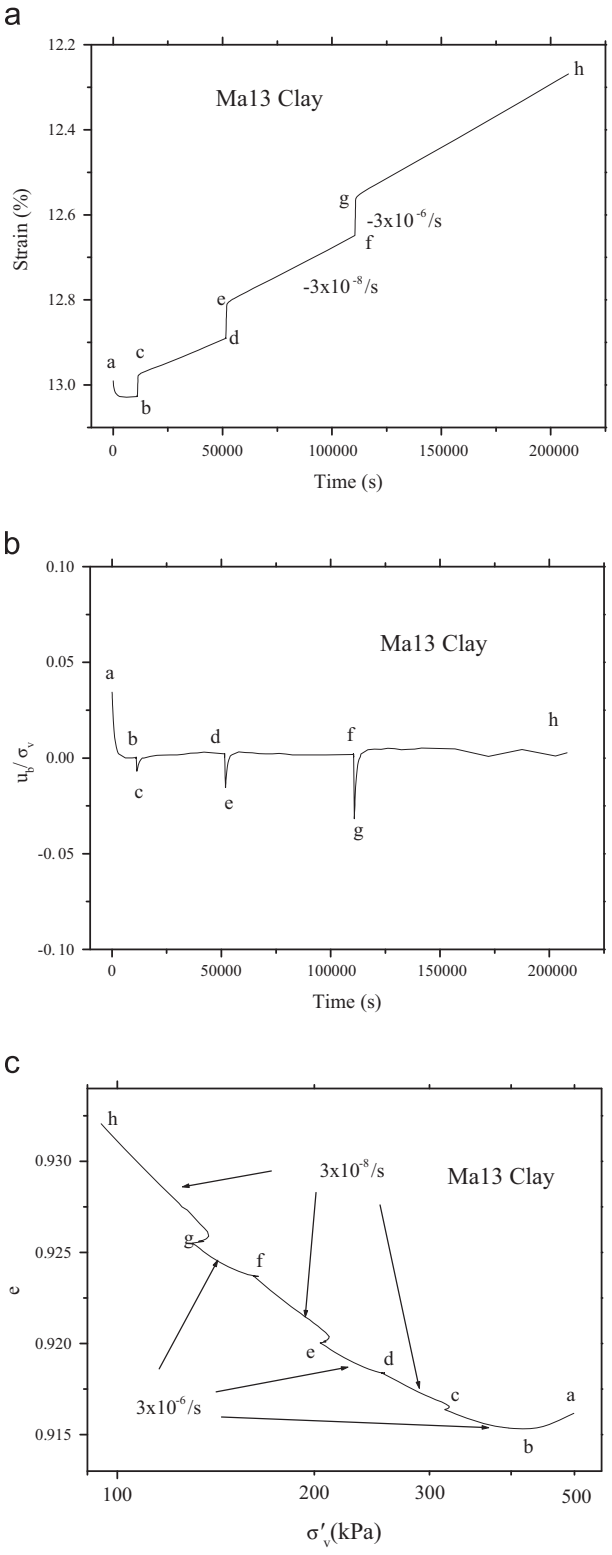

Fig. 13. Influence of the strain rate on the e–log σ'_v relation during the unloading test (Ma13 Clay). (a) Time vs strain, (b) time vs pore pressure, and (c) e–log p relation at different strain rates.

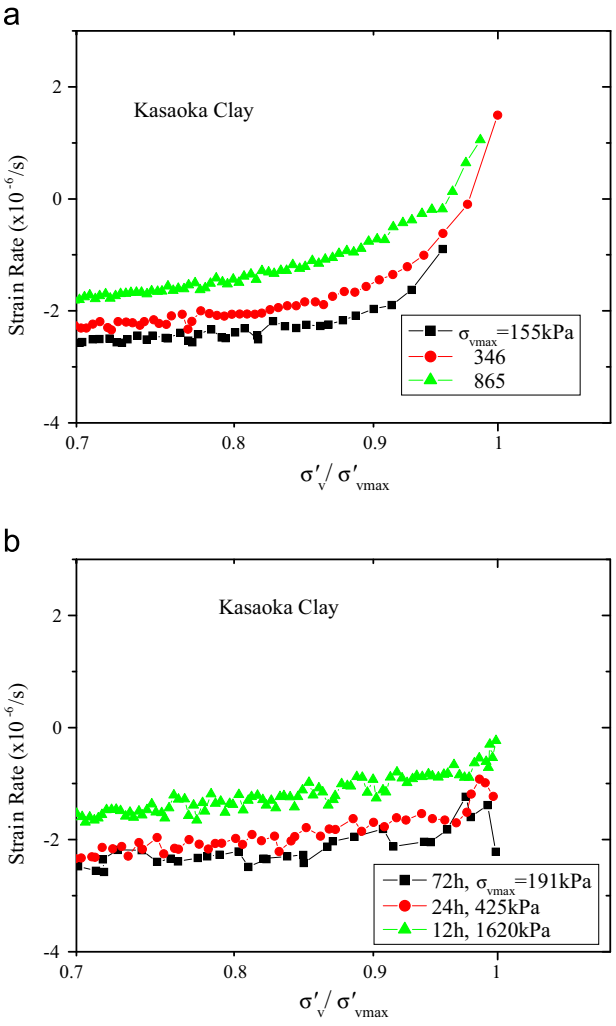

Fig. 14. Strain rates at the unloading test for Kasaoka clay. (a) No creep. Corresponding to Fig. 6(a). (b) After creep. Corresponding to Fig. 10(a).

unloading test. For tests without the constant loading, the strain rates were far larger than the intended rate (-3×10^{-6}/s) at the very early stages of the unloading, i.e., at large σ'_v/σ'_{vmax}, but they became stable at σ'_v/σ'_{vmax} smaller than 0.9 even though the strain rate was still slightly decreasing. In addition, it should be noted that this tendency becomes prominent especially when the applied load is large ($\sigma_{vmax}=865$ kPa) due to the large deformation of the load cell. Therefore, strictly speaking, the strain rate is not constant for different values of σ'_v/σ'_{vmax} and load levels. However, as is shown in a later section of this paper, the strain rate dependency under the unloading can be recognized only by change in the order of 1/10 or 1/100 so that the discrepancy in the strain rate observed in Fig. 14 may be ignored. It is interesting to note that the strain rate of the specimen subjected to creep is more stable than that without creep. This is because the specimen became stiffer due to creep.

After the a and b process, the strain rate alternatively increased to -3×10^{-6}/s (b and c, d and e, f and g) or decreased to -3×10^{-8}/s (c and d, e and f, g and h for only Ma13 clay), as seen in Figs. 12 and 13. The response of u_b in the form of u_b/σ_v is also plotted in these figures. Negative u_b/σ_v is developed at the fast strain rate, but when the strain rate was slower, u_b/σ_v gradually dissipated, and in the process, u_b/σ_v was nearly zero.

Except at the early stage, a strain rate dependency was clearly observed even in the unloading process; i.e., as the strain rate slowed, the e–log σ'_v relation shifted to the right, and this tendency was significant at smaller values of σ'_v (compare the change at c, e and g in Fig. 13 (c)). In addition, the effect of changing the strain rate on the e–log σ'_v relation is much more prominent during the transition from fast to slow strain rates than that from slow to fast rates (for example, compare e and f in Fig. 13(c)).

To observe the e–σ_v relation during the transition of the strain rate in more detail, the points e and f for Kasaoka clay in Fig. 12(c) are enlarged in Fig. 15. Fig. 15(a) presents the point e, where the unloading test was carried out at -3×10^{-6}/s and changed to -3×10^{-8}/s, while Fig. 15 (b) shows the point f, which is the reverse case of e. In these figures, the e–σ_v relation is plotted by both of σ_v and σ'_v. At the small strain rate, because of the small u_b and i, the values of σ'_v and σ_v are nearly the same, while some difference between the values of σ_v and σ'_v was detected at the fast strain rate. Since negative u_b is generated under the unloading conditions, σ'_v becomes larger than σ_v. That is, the strain rate dependency is less significant if it is evaluated in terms of σ'_v, which is calculated assuming that the pore water pressure distribution is a cubic polynomial, as mentioned earlier.

Immediately after changing the strain rate from -3×10^{-6}/s to -3×10^{-8}/s, the values of both σ_v and σ'_v increased, but soon decreased again (see Fig. 15(b)). To study this strange behavior, the observed strain and the values of σ_v and σ'_v are plotted against elapsed time in Fig. 16, where (a) and (b) are the same figures but with a different time scale. The strain rate was changed at the point marked e_1, and the next measured point was e_2. Before e_1, including this point, σ'_v was calculated assuming that the coefficient of α in Eq. (13) is -1, because the absolute strain rate for the loading test measuring u_o is the same as that for the unloading test, with different signs for positive and negative. From e_2, however, the value of σ'_v was calculated without considering the influence of i (the α is -0.01). Therefore, as seen in Fig. 15(a), the difference between σ_v

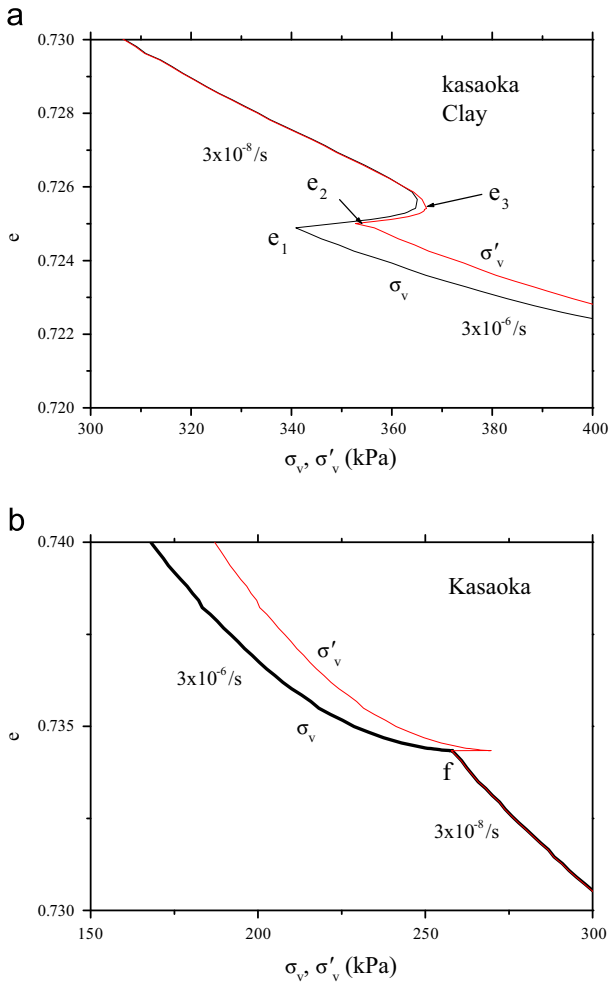

Fig. 15. Magnified e–σ'_v and e–σ_v relation at a changing strain rate. Note that σ'_v and σ_v are plotted in arithmetic scale. (a) At e (from a high strain rate to a low strain rate), (b) at f (from a low strain rate to a high strain rate).

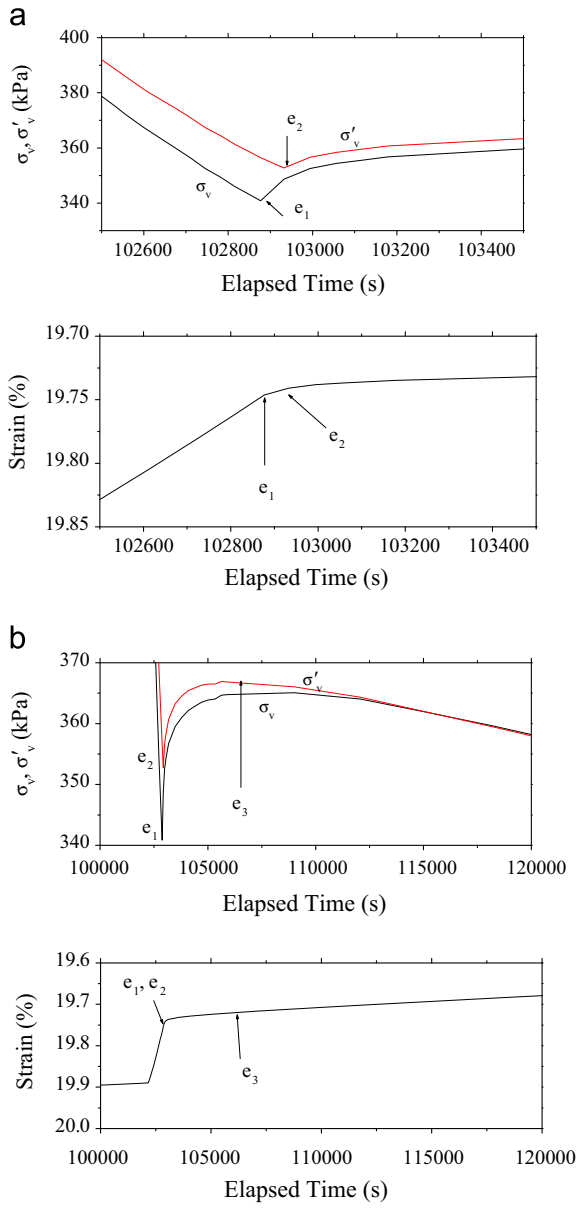

Fig. 16. Detailed performance of pressures and strain to the time. (a) At e_1 and e_2, (b) at e_3.

and σ'_v became small after the e_2 point, but a difference remains until the complete dissipation of the negative u_b generated by the previous unloading test under a relatively high strain rate. If measurements at times before e_2 were taken, and the σ'_v values were calculated at these points, then the e–σ'_v relation around the e_2 point might be somewhat different. The same may be true of point f in Fig. 15 (b), where a spike of σ'_v is observed. Before the f point, σ'_v is calculated by $\alpha=0$, but after f, α is suddenly "-1".

As mentioned earlier, the values of σ'_v and σ_v increase from e_1 or e_2 and they gain the maximum stress at e_3 before decreasing again. As seen in Fig. 16 (b), the strain increased very smoothly with time, which is also true at e_3 and the values of σ_v and σ'_v gradually approach the same value according to the u_b dissipation, without any special events. It is evident that this strange behavior is not caused by discontinuities of the strain and time relation. The same phenomenon is observed in the loading test at the NC state, i.e., the stress reduction is more clearly observed as the strain rate decreased than the stress increase as the strain rate increased (Tsutsumi and Tanaka, 2011, 2012). It is possible that these behaviors can be explained by differences in the excess pore water pressure generated in the specimen, or by differences in the visco properties, but further research is required to determine the cause.

5. Comparison with constant loading test

As already mentioned, unloading behavior is usually studied by the constant load test, where the load is instantaneously removed and displacement is measured under the constant load. In this study, the unloading behavior was also studied by the constant load test for Ma 13 clay. The test was carried out following the JIS A 217:2009, where the specimen is 60 mm in diameter and 20 mm in initial height. Both the upper and lower sides of the specimen were kept in the drainage condition. After the specimen was consolidated under a consolidation stress of 90 kPa for 24 h (the preconsolidation stress of the specimen was 100 kPa), a consolidation stress of 330 kPa (σ_{vmax}) was applied for 2 h before the stress was removed to prescribed σ_v/σ_{vmax} levels. One of the reasons for the relatively short time of 2 h consolidation time is to simulate the same condition as the CRS test in the present study, i.e., the order of $\dot{\varepsilon}$ should be equivalent to 2.8×10^{-6}/s, which is the same order of the strain rate in the loading before the unload for the CRS test in this study. However, $\dot{\varepsilon}$ at 2 h was somewhat slower than 2.8×10^{-6}/s. This point will be discussed in more detail in a later section of this paper.

Changes in e during the unloading test (Δe) are plotted against the elapsed time in Fig. 17. It is well known that when the removal stress is smaller than the intensity of the consolidation stress, i.e., large σ_v/σ_{vmax} in this study, the decrease in e is again observed after a certain time (compression). In this study, such behavior is seen even when σ_v/σ_{vmax} of 0.79. It should be kept in mind that this stress ratio is rather small compared with that cited in previous research where the duration of the loading before the

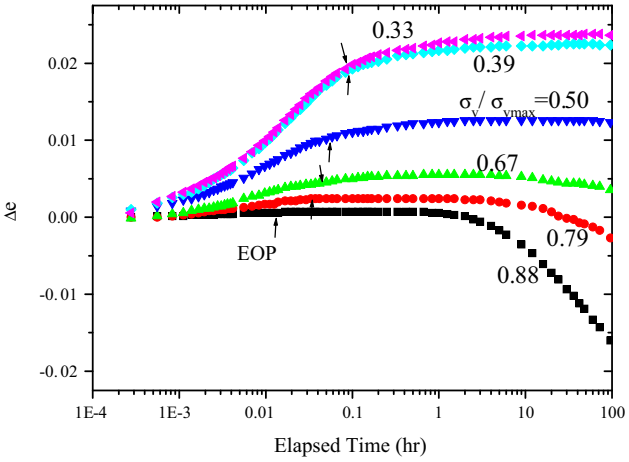

Fig. 17. Relationship between Δe and elapsed time measured by constant load test.

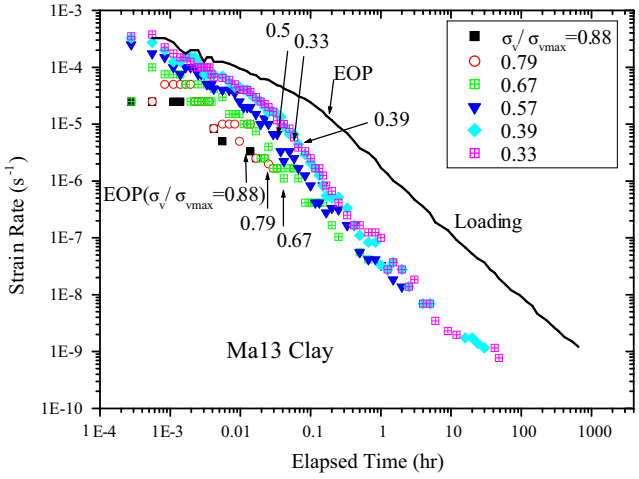

Fig. 18. Strain rates from loading and unloading tests. Note that the strain rate in the figure is absolute value (in case of the loading, positive, but in case of the unloading, negative).

removal is much longer; in another words, the value of $\dot{\varepsilon}$ was much smaller.

The strain rate for the unloading test is presented in Fig. 18, together with the relation measured in the loading test at the NC state. These relations are plotted in the same figure for the purpose of easy comparison, with the absolute values of the strain rate plotted on the vertical axis. When we see the relation between the elapsed time and the strain rate for the Loading test (indicated by the solid line in Fig. 18), the strain rate at 2 h was about 8×10^{-7}/s, which is slightly slower than the intended rate of $2.8-10^{-6}$/s. Nevertheless, if the duration is much shorter than 2 h, the amount of error in the time required for the removal load influences the test results considerably and there is a possibility that a large amount of the excess pore water pressure remains in the specimen. In these loading and unloading tests under constant (total) stress, the pore water pressure was not measured. The time of the EOP was estimated by the Cassagrande method, i.e., $\sqrt{t}$ method. The time at EOP is indicated by arrows in Figs. 17 and

18. Although there was a tendency that the time at EOP increased with a decrease in σ_v/σ_{vmax}, primary consolidation was attained after 0.1 h (6 min) for all unloading tests. The elapsed time at $\dot{\varepsilon}$ of -2.8×10^{-6}/s, which is the standard strain rate for the unloading test in this study, was dependent on the σ_v/σ_{vmax} level, in the same way as the time at EOP. The time required to reach $-2.8-10^{-6}$/s was around 0.015 h (1 min) when σ_v/σ_{vmax}=0.88 and 0.1 h (6 min) when σ_v/σ_{vmax}=0.33, which was much shorter than the times required in the loading case (about 1 h) and nearly the same as the times required when the pore water pressure was dissipated (EOP). The time required for an $\dot{\varepsilon}$ of -2.8×10^{-8}/s, which is the slowest rate in the present study, was 1 h or 2 h after the load was removed. When the constant load test for unloading was carried out following the conventional constant load test with 24 h of duration at each unloading stage, the order of $\dot{\varepsilon}$ is considerably small, at approximately -10^{-9}/s.

The relations of Δe–σ'_v/σ'_{vmax} measured by the CRS and the constant load tests are compared in Fig. 7(c). These relations are in good agreement with each other and a notably small strain rate dependency occurred at small σ'_v/σ'_{vmax} in both sets of results. This indicates that even in the unloading condition, the soil behavior is controlled by the strain rate in the same way as it is in the loading behavior (see, for example, Leroueil et al., 1985). However, this conclusion seems somewhat premature given that only one clay sample was used in this study.

Another comparison is shown in Fig. 19, where the Δe–σ'_v/σ'_{vmax} relation is presented in terms of C_s and the data for the constant loading are obtained from Mesri et al. (1978). Crushed or slaked shale was used as the test materials in their study, and the sample used to produce the results used in this figure was Bearpaw shale with Atterberg limits of w_L 110% and w_P 22%. The duration of σ'_{vmax} was the same as when 99% of the excess pore water pressure was dissipated when measured at the bottom. Although their C_s is larger than that in the present study, the non-linearity observed for C_s against σ'_v/σ'_{vmax} is similar. In addition, it is worth noting that the same C_s and σ'_v/σ'_{vmax} relation was measured for σ'_{vmax} of 551 kPa and 3445 kPa. This implies that even in the constant unloading test, the Δe–σ'_v/σ'_{vmax} relation is not affected by the intensity of σ'_{vmax}.

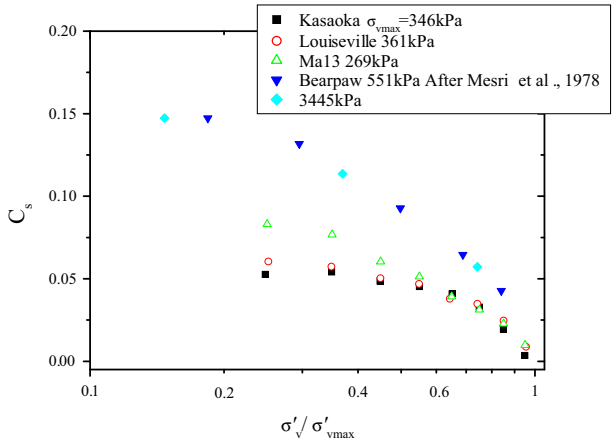

Fig. 19. C_s measured by the present study (CRS) and Mesri et al. (1978) (Constant Loading).

6. Conclusions

The unloading behavior of clays has been investigated by the CRS test and compared with that measured by the constant load test. In order to calculate the effective stress in the CRS test, the distribution of the excess pore water pressure during the unloading was simulated by a cubic polynomial equation. The validity of this simulation was examined by an FEM analysis. The most interesting and important findings in this study are as follows:

(1) A unique relation between Δe and σ'_v/σ'_{vmax} was found, irrespective of the intensity of σ'_{vmax}, where σ'_{vmax} is the σ'_v before unloading test (the maximum stress) and Δe is the void ratio increment from e at σ'_{vmax}. This finding was also applied to Louiseville clay, which exhibits a strong non-linearity of the e–log σ'_v relation. That is, the swelling index (C_s) is not influenced by the compression index (C_c).
(2) The Δe–log σ'_v/σ'_{vmax} relation is notably non-linear indicating that C_s is affected by the intensity of the swelling stress. This non-linearity is the same as that measured by the constant loading test.
(3) The duration of consolidation under the constant load before the unloading, in another words, the amount of creep strain, was shown to have an effect on the Δe–log σ'_v/σ'_{vmax} relation. Large creep strain stiffens the soil; i.e., C_s becomes smaller.
(4) A strain rate dependency was observed for the Δe–σ'_v relation under unloading, which became significant at small σ'_v/σ'_{vmax} ratios.

References

Kawaguchi, T., Tanaka, H., 2008. Formulation of G_{max} from reconstituted clayey soils and its application to G_{max} measured in the field. Soils Found. 48 (6), 821–832.
Leroueil, S., Kabbaj, M., Tavenas, F., Bouchard, R., 1985. Stress–strain–strain rate relation for the compressibility of sensitive natural clays. Geotechnique 35, 159–180.
Leroueil, S., 1997. Geotechnical characteristics of Eastern Canada clays. In: Proceedings of the International Symposium on Characterization of Soft Marine Clays, Bothkennar, Drammen, Quebec and Ariake Clays, Yokosuka, Japan, AA Balkema, pp. 3–32.
Mesri, G., Ullrich, C.R., Choi, Y.K., 1978. The rate of swelling of overconsolidation clays subjected to unloading. Geotechnique 28 (3), 281–307.
Mitachi, T., Kitago, S., 1976. Change in undrained shear strength characteristics of saturated remolded clay due to swelling. Soils Found. 16 (1), 45–58.
Moriwaki, T., Umehara, K., 2003. Method for determining the coefficient of permeability of clays. Geotech. Test. J. 26 (1), 1–10.
Ohta, H., Nishimura, A.,Morita, Y., 1985. Undrained stability of Ko-consolidated clays, Proceedings of 11th ICSMFE, vol. 2, pp. 613–616.
Shinohe, A., Nishimura, S., 2012. High-accuracy evaluation of soils' one-dimensional compressibility by image analysis. In: Proceedings of the 47th Japan National Conference on Geotechnical Engineering, pp. 583–584 (in Japanese).

Tanaka, H., 2005. Consolidation behavior of natural soils around pc value – long term consolidation test. Soils Found. 45 (3), 83–96.
Tanaka, H., Shiwakoti, D.R., Mishima, O., Watabe, Y., Tanaka, M., 2001. Comparison of mechanical behavior of two overconsolidated clays: Yamashita and Louiseville clays. Soils Found. 41 (4), 73–88.
Tsutsumi, A., Tanaka, H., 2011. Compressive behavior during the transition of strain rate changing. Soils Found. 51 (5), 813–822.
Tsutsumi, A., Tanaka, H., 2012. Combined effects of strain rate and temperature on consolidation behavior of clayey soils. Soils Found. 52 (2), 210–218.
Watabe, Y., Udaka, K., Morikawa, Y., 2008. Strain rate effect on long term consolidation of Osaka bay clay. Soils Found. 48 (4), 495–509.
Wood, D.M., 1990. Soil Behaviour and Critical State Soil Mechanics. Cambridge University Press.